Optimal Control and Estimation Techniques for Reaction Wheel Inverted Pendulum(RWIP)

Basharat Shafi(24310019), Divij Yadav(24270003), Yash Kashiv(24250108)
Indian Institute of Technology Gandhinagar
Gandhinagar, Gujarat, India
Email:24310019@iitgn.ac.in, 24270003@iitgn.ac.in, 24250108@iitgn.ac.in

***Abstract*—The Reaction Wheel Inverted Pendulum (RWIP) presents a classic underactuated, nonlinear control problem requiring precise strategies for stabilization. This work introduces a hybrid control framework that combines an energy-based swing-up controller with linear stabilizers to achieve upright balance. The swing-up phase injects energy to drive the pendulum into a $\pm 15^\circ$ band near vertical. Once within this range, four stabilization strategies are compared: Pole Placement, Linear Quadratic Regulator (LQR), Luenberger Observer-based control, and LQR with Kalman Filter (LQG). Among them, LQR achieves the fastest 2% settling time of $0.90\,$s, outperforming Pole Placement by 18%, while LQG ensures robust state estimation, reducing error by 98% within $0.35\,$s. This study offers a modular design integrating estimation and control, with simulation results highlighting trade-offs in speed, robustness, and complexity. Overall, LQR emerges as the most effective choice for balancing control performance and implementation efficiency in underactuated systems.**

***Index Terms*—Reaction Wheel Inverted Pendulum (RWIP), Hybrid Control, Energy-Based Swing-Up, Pole Placement, Linear Quadratic Regulator (LQR), Luenberger Observer, Kalman Filter, State Estimation, Stabilization, Underactuated Systems.**

I. Introduction

The Reaction Wheel Inverted Pendulum (RWIP) is a canonical problem in control engineering, characterized by underactuation and nonlinear dynamics [1], [2]. It models a pendulum mounted on a rotating wheel and serves as a benchmark for testing modern control techniques in applications such as robotics, aerospace systems, and precision balancing platforms [3].

This study addresses two key challenges: first, using energy-shaping to swing the pendulum from its downward equilibrium to near-upright [4]; and second, maintaining balance through linear feedback once within a $\pm 15^\circ$ region [5]. Although various control methods have been applied to RWIP systems, a comparative analysis across state-feedback and observer-based strategies remains limited [6].

We implement a hybrid architecture comprising a nonlinear swing-up controller followed by four stabilization strategies: Pole Placement [7], LQR [5], Luenberger Observer [8], and Kalman Filter. Each method is evaluated based on its stabilization time, overshoot, and control effort. The LQR strategy minimizes a performance cost function [9], while observer-based approaches estimate states under noisy conditions [7].

Key contributions include:

- A unified framework integrating swing-up and stabilization phases [2],
- Quantitative analysis of multiple control strategies through simulation [10],
- Validation of Kalman Filter performance under noisy measurements [5].

The remainder of the paper is structured as follows: Section II covers RWIP dynamics and linearization [1]. Section III discusses controllability and observability [7]. Sections IV and V describe controller design [11]. Section VI presents results and comparison [**?**], followed by conclusions in Section VII.

II. System Description

The system consists of a vertical rod (the **pendulum**) that is mounted on a fixed base. Attached to the top of this pendulum is a **reaction wheel**, which is a rotating disc capable of spinning around its own horizontal axis [2].

The primary goal is to maintain the pendulum in the upright position, despite this being an inherently unstable configuration [3]. The **reaction wheel** serves as the only actuator in the system. By accelerating or decelerating the spin of the wheel, it produces a reaction torque that acts on the pendulum, thereby influencing its angular position [1].

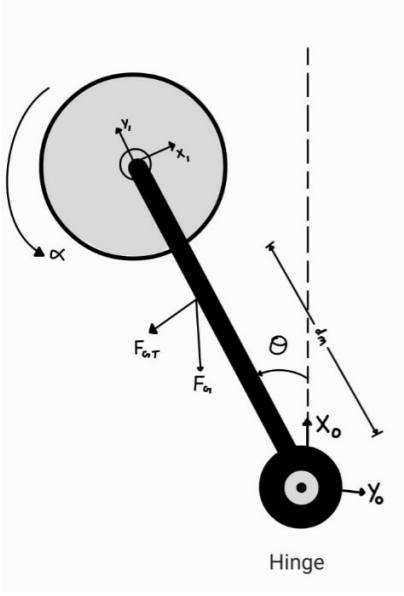

Fig. 1. Inverted Pendulum with Reaction Wheel

- The angle θ represents the tilt of the pendulum from the vertical upright position. When $\theta = 0$, the pendulum is perfectly vertical
- The angle α describes the angular position of the reaction wheel relative to the pendulum.
- The center of mass of the pendulum is located at a distance d^M from the base.
- Gravitational forces act on both the pendulum and the reaction wheel, pulling them downward.
- The system is mounted such that the base is fixed, and the only means of actuation is through the spinning of the reaction wheel.

This setup represents a classic example of an **underactuated** and **nonlinear** control system [12]. Such systems are commonly found in applications like spacecraft attitude control, robotics, and other domains where precision stabilization of unstable configurations is critical [13].

A. Mathematical Model

The system dynamics of the Reaction Wheel Inverted Pendulum (RWIP) can be described through its nonlinear equations of motion. These are derived using principles of rigid body dynamics, including the effects of friction, torque inputs, and motor dynamics [10].

a) Nonlinear Model:: The nonlinear model governing the pendulum angle θ and the wheel rotation angle α is [9]:

$$\ddot{\theta} = \frac{M_p d_M g}{J}\sin(\theta) - \frac{b_\theta}{J}\dot{\theta} + \frac{b_\alpha}{J}\dot{\alpha} + \frac{1}{J}\tau_d - \frac{1}{J}\tau_w, \quad (1)$$

$$\begin{aligned}\ddot{\alpha} = &-\frac{M_p g d_M}{J}\sin(\theta) + \frac{b_\theta}{J}\dot{\theta} - \frac{(J+J_w)b_\alpha}{JJ_w}\dot{\alpha} \\ &- \frac{1}{J}\tau_d + \frac{(J+J_w)}{JJ_w}\tau_w \end{aligned} \quad (2)$$

where the variables represent:

- M_p – mass of the pendulum and reaction wheel combined,
- d_M – distance from the axis z_0 to the center of mass,
- g – gravitational acceleration,
- J – total moment of inertia of the pendulum system,
- J_w – moment of inertia of the wheel,
- b_θ, b_α – friction coefficients for θ and α,
- τ_d – disturbance torque,
- τ_w – torque applied by the reaction wheel.

III. Approximated Mathematical Modeling

A. Overview and Theoretical Background

This section outlines the modeling of the reaction-wheel inverted pendulum (RWIP), which uses a motor-driven wheel to stabilize the pendulum in its upright position [14]. The model captures the coupled dynamics of the pendulum and wheel, incorporating nonlinearities and disturbances. ... We first wrote [6] the full nonlinear equations using Lagrange's method. Then, we apply simplifying assumptions and linearize the model about the upright equilibrium [11]. The resulting equations are expressed in state-space form for control design [7].

The section includes: nonlinear dynamics equations, linearization, state-space formulation, key parameters, and a brief note on model limitations.

B. Nonlinear Equations of Motion

The complete nonlinear equations governing the dynamics of the reaction-wheel inverted pendulum about the upward unstable equilibrium are presented in Equation (2). These expressions capture the coupled motion of the pendulum angle and the reaction wheel, accounting for gravitational, damping, and motor-related effects in a nonlinear framework [1].

C. Simplifying Assumptions for Control Design

To obtain a tractable model suitable for control design, several simplifying assumptions are made [15]. These assumptions reduce the complexity of the nonlinear equations while preserving the essential dynamics of the system:

1) **Negligible Disturbance Torque:** External disturbances are assumed to be negligible, i.e., $\tau_d \approx 0$, to focus on the core dynamics.
2) **Rigid Pendulum Approximation:** The pendulum is modeled as a rigid rod of length L with its center of mass (COM) at $L/2$, leading to the moment of inertia:
$$J_p = \frac{1}{3}m_p L^2,$$
where m_p is the pendulum mass....
3) **Solid-Disk Reaction Wheel:** The reaction wheel is approximated as a solid disk of radius r, resulting in the moment of inertia:
$$J_w = \frac{1}{2}m_w r^2,$$
where m_w is the wheel mass.
4) **Reduction of State Variables:** The original model may consider four states, including θ, $\dot{\theta}$, α, and $\dot{\alpha}$, to fully describe the system dynamics. However, for control design purposes, the state vector is reduced to three states: θ, $\dot{\theta}$, and $\dot{\alpha}$ [2]. This reduction is justified by the fact that the absolute angle of the reaction wheel α does not directly affect the pendulum's stability or the control torque applied via the wheel's angular velocity. Ignoring α simplifies the state-space representation without compromising the ability to stabilize the pendulum in the upright position.

Under these assumptions, the simplified nonlinear equations of motion become [6]:

$$\begin{aligned}\ddot{\theta} &= \frac{(m_p + m_w)gL\sin\theta - b_p\dot{\theta} + u}{J_p}, \\ \ddot{\alpha} &= \frac{-b_w\dot{\alpha} - u}{J_w},\end{aligned} \quad (3)$$

where b_p and b_w are the effective damping coefficients for the pendulum and wheel, respectively, and u represents the control torque.

D. Linearization About the Upright Equilibrium

For control design purposes, particularly for linear control techniques such as LQR, the nonlinear equations are linearized about the upright equilibrium position, where $\theta = 0$ [9]. At this point, the approximation $\sin\theta \approx \theta$ holds for small angles. Applying this approximation to Equation (3), the linearized dynamics are:

$$\begin{aligned} \ddot{\theta} &\approx \frac{(m_p + m_w)gL}{J_p}\theta - \frac{b_p}{J_p}\dot{\theta} + \frac{1}{J_p}u, \\ \ddot{\alpha} &\approx -\frac{b_w}{J_w}\dot{\alpha} - \frac{1}{J_w}u. \end{aligned} \tag{4}$$

These equations represent the system behavior near the upright position and are suitable for designing controllers that stabilize the pendulum in this unstable equilibrium [11].

E. State-Space Representation

To facilitate modern control design, the linearized equations are cast into state-space form [7]. Define the state vector x and the control input u as:

$$x = \begin{bmatrix} \theta & \dot{\theta} & \dot{\alpha} \end{bmatrix}^{\mathsf{T}}, \quad u = \text{control torque}.$$

The state-space model is then expressed as:

$$\dot{x} = Ax + Bu, \quad y = Cx, \quad D = 0,$$

where the system matrices are [11]:

$$A = \begin{bmatrix} 0 & 1 & 0 \\ \frac{(m_p+m_w)gL}{J_p} & -\frac{b_p}{J_p} & -\frac{b_w}{J_p} \\ ...0 & 0 & -\frac{b_w}{J_w} \end{bmatrix}, \quad B = \begin{bmatrix} 0 \\ \frac{1}{J_p} \\ -\frac{1}{J_w} \end{bmatrix},$$

C = $\mathrm{I}_{3\times 3}$.

This representation allows for the application of state-space control techniques and provides a compact form for simulation and analysis [16].

F. System Parameters

The numerical values of the system parameters used in the model are summarized in Table I. These values are based on physical measurements or manufacturer specifications and are critical for accurate simulation and control design [6].

Parameter	Symbol	Value	Units
Pendulum mass	m_p	0.20	kg
Wheel mass	m_w	0.30	kg
Pendulum length	L	0.70	m
Wheel radius	r	0.08	m
Gravitational acceleration	g	9.81	m/s^2
Pendulum inertia	J_p	$\frac{1}{3}m_pL^2 \approx 0.0327$	kg·m^2
... Wheel inertia	J_w	$\frac{1}{2}m_wr^2 \approx 0.00096$	kg·m^2
Pendulum damping	b_p	0.02	N·m·s/rad
Wheel damping	b_w	0.005	N·m·s/rad

TABLE I
NUMERICAL VALUES OF THE RWIP SYSTEM PARAMETERS.

IV. System Analysis

This section examines the controllability, observability, and open-loop stability of the linearized Reaction Wheel Inverted Pendulum (RWIP) model about the upright equilibrium [7]. All computations were performed in MATLAB using the `ctrb`, `obsv`, and `eig` functions on the matrices A and B defined in Appendix .

A. Controllability

Controllability determines whether the control input can transfer the system between arbitrary states [11]. For the linear state-space realization

$$\dot{x} = Ax + Bu,$$

the controllability matrix is

$$\mathcal{C} = \begin{bmatrix} B & AB & A^2B \end{bmatrix}.$$

In MATLAB, `rank(ctrb(A,B))` returns

$$\operatorname{rank}(\mathcal{C}) = 3,$$

which equals the system order. Hence, the RWIP model is *fully controllable*, implying that all states θ, $\dot{\theta}$, and $\dot{\alpha}$ can be driven by the reaction wheel torque [7].

B. Observability

Observability assesses whether the full state can be reconstructed from the output [8]. With output equation

$$y = Cx,$$

the observability matrix is

$$\mathcal{O} = \begin{bmatrix} C \\ CA \\ CA^2 \end{bmatrix}.$$

Evaluating `rank(obsv(A,C))` in MATLAB yields

$$\operatorname{rank}(\mathcal{O}) = 3,$$

indicating that the system is *fully observable* [7]. Thus, a suitable observer (e.g., a Kalman filter) can estimate $\dot{\theta}$ and $\dot{\alpha}$ from measurements of θ (and any additional outputs).

C. Open-Loop Stability

The eigenvalues of A characterize the inherent stability [16]:

$$\lambda = \operatorname{eig}(A) \approx \{\, 9.9506,\ -10.5629,\ -5.2083 \}.$$

One eigenvalue has positive real part (9.9506), while the other two are negative. Therefore, the upright equilibrium is *unstable* in open-loop, with a single unstable mode corresponding to the pendulum's tendency to fall [3].

D. Stabilizability

Although the system is open-loop unstable, it is stabilizable because [9]:

- The unstable mode is reachable (it appears in the controllable subspace).
- Full controllability guarantees that state feedback can relocate all poles.

Consequently, a state-feedback controller (e.g., via pole placement or LQR) can shift the unstable eigenvalue into the left half-plane, achieving closed-loop stability [11].

TABLE II
SUMMARY OF LINEAR SYSTEM PROPERTIES

Property	Result
Controllability rank	3 (full)
Observability rank	3 (full)
...	
Number of states	3
Open-loop eigenvalues	$9.9506, -10.5629, -5.2083$
Open-loop stability	Unstable (one positive eigenvalue)

V. CONTROLLER DESIGN FOR RWIP STABILIZATION (HYBRID CONTROL STRATEGY)

This section presents a hybrid control strategy for stabilizing the Reaction Wheel Inverted Pendulum (RWIP) [14]. The approach starts with swing-up control to move the pendulum from the downward to near-upright position. Once the pendulum angle is within 15° of the upright equilibrium, control switches to a stabilizing controller to maintain balance [4]. The following subsections describe the swing-up mechanism and the subsequent stabilizing controllers in detail.

A. Swing-Up Control for Initial Motion

The swing-up control transitions the pendulum from the downward position ($\theta = \pi$ radians) to the upright position ($\theta = 0.2618$ radians) by injecting energy into the system [17]. This serves as the initial stage for all subsequent stabilizing controllers.

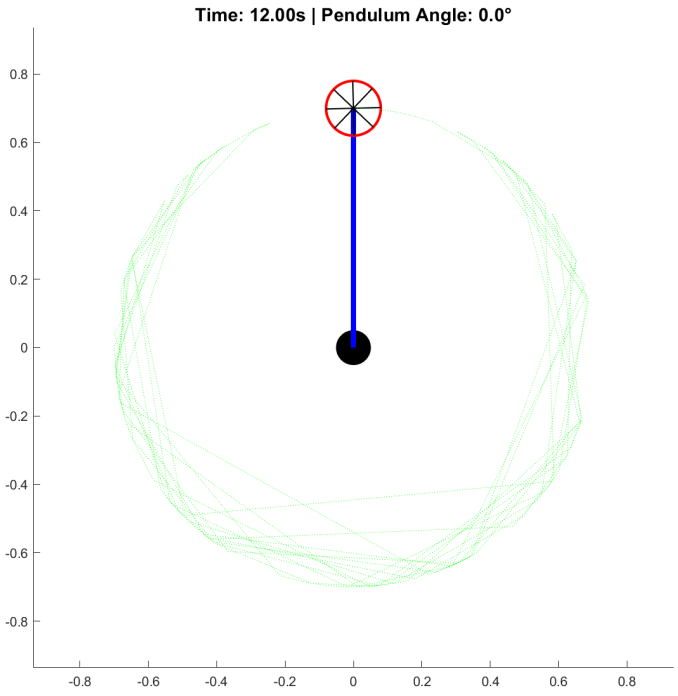

Fig. 2. Trajectory of the pendulum tip during swing-up and stabilization. The green dashed line traces the path followed by the pendulum end-effector, while the pendulum is shown upright at the final stabilized configuration.

The desired energy to reach the upright position is given by [18]:

$$E_{\text{desired}} = 2(m_p + m_w)gL, \tag{5}$$

where m_p is the pendulum mass, m_w is the wheel mass, g is gravitational acceleration, and L is the pendulum length.

The current energy at any time is:

$$E_{\text{current}} = \frac{1}{2}J_p\dot{\theta}^2 - (m_p + m_w)gL\cos\theta, \tag{6}$$

where J_p is the moment of inertia and $\dot{\theta}$ is the angular velocity.

The control torque u is formulated as [4]:

$$u = k_E(E_{\text{desired}} - E_{\text{current}})\dot{\theta} + k_\theta(\pi - \theta)\dot{\theta}, \ldots \tag{7}$$

with $k_E = 3.5$ and $k_\theta = 4$ as the tuning parameters. To prevent actuator saturation:

$$u = \text{sign}(u) \cdot \min(|u|, u_{\text{max}}), \tag{8}$$

where $u_{\text{max}} = 1.0\,\text{Nm}$.

The swing-up control continues until the pendulum angle θ is within $\pm 15°$ of the upright position. At this point, the system transitions to one of the stabilizing controllers [6].

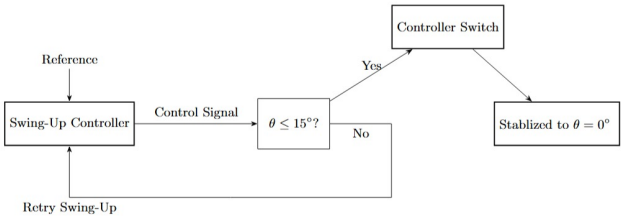

Fig. 3. Control system block diagram for Reaction Wheel Inverted Pendulum with switching mechanism to stabilizing controller.

B. Stabilization Controllers for Upright Equilibrium

Once the pendulum angle is within $\pm 15^\circ$ of the upright position, the control strategy switches to a stabilizing controller to maintain the pendulum at $\theta = 0$ [14]. This subsection outlines the stabilizing control methods based on the linearized RWIP model around the upright equilibrium. These feedback controllers aim to move the system's unstable pole to the left-half plane of the complex plane [16]. The following subsubsections describe the specific stabilizing techniques, which can be integrated into the hybrid control after the swing-up phase.

1) Pole Placement Method: The Pole Placement method stabilizes the RWIP system by placing the closed-loop poles at desired locations in the complex plane once the pendulum angle is within $\pm 15^\circ$ of the upright position [7].

Given the linearized state-space model:

$$\dot{x} = Ax + Bu, \tag{9}$$

the state feedback controller is designed as:

$$u = -K(x - x_{\text{ref}}), \tag{10}$$

where K is the feedback gain matrix, and $x_{\text{ref}} = [0, 0, 0]^T$ is the reference state. The desired poles are chosen as:

$$\text{Desired Poles} = [-12, -15, -17], \tag{11}$$

to ensure stability and fast response. The gain matrix K is computed using MATLAB's `place` function [11]. This controller is active when $|\theta| \leq 15^\circ$, providing stabilization near the upright position.

2) Linear Quadratic Regulator (LQR) Approach: The Linear Quadratic Regulator (LQR) stabilizes the RWIP system once the pendulum angle is within $\pm 15^\circ$ of the upright position [5]. It minimizes a quadratic cost function balancing state deviation and control effort.

Given the linearized state-space model:

$$\dot{x} = Ax + Bu, \tag{12}$$

the LQR controller is designed as:

$$u = -K(x - x_{\text{ref}}), \tag{13}$$

where K is the optimal feedback gain matrix, and $x_{\text{ref}} = [0, 0, 0]^T$ is the reference state. The cost function is [5]:

$$J = \int_0^\infty \left(x^T Q x + u^T R u\right) dt, \tag{14}$$

where Q and R are the state and control weighting matrices, respectively. For the RWIP system:

$$Q = \text{diag}(100, 10, 0.1), \quad R = 0.1, \tag{15}$$

The optimal gain matrix K is computed using MATLAB's `lqr` function. This approach relocates the system's unstable poles and stabilizes the pendulum [6].

The LQR controller is active when $|\theta| \leq 15^\circ$, providing robust and optimal stabilization of the pendulum at the upright position.

The overall control structure used for both the Pole Placement and LQR methods is shown in Figure 4. This block diagram represents a standard full-state feedback system, where the measured state vector x is fed back through the gain matrix K to compute the control input u.

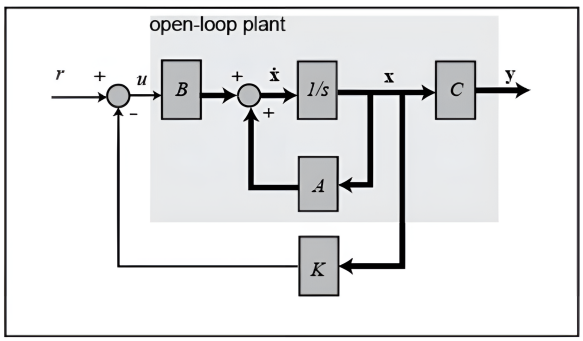

Fig. 4. Full-state feedback control block diagram used in both Pole Placement and LQR methods. The structure remains identical; only the gain matrix K differs based on the design method.

In both cases, the same system architecture is used, with the gain matrix K computed differently:

- For **Pole Placement**, K is determined by assigning the desired closed-loop poles directly using pole placement techniques.
- For **LQR**, K is computed by minimizing a quadratic cost function balancing state errors and control effort.

This unified block diagram reinforces the modularity and flexibility of the control approach: once a reliable state-space model is established, the specific controller can be tuned by simply updating the feedback gain.

3) Luenberger Observer for State Estimation: ... The Luenberger Observer estimates the states of the RWIP system from incomplete measurements [8], crucial during the stabilizing phase when the pendulum angle is within $\pm 15^\circ$ of the upright position, ensuring accurate feedback for control.

Given the linearized state-space model:

$$\dot{x} = Ax + Bu, \quad y = Cx, \tag{16}$$

where $x = [\theta, \dot{\theta}, \dot{\alpha}]^T$ is the state vector, y is the output, A, B, and C are system matrices, and u is the control torque, the observer dynamics are [7]:

$$\dot{\hat{x}} = A\hat{x} + Bu + L(y - C\hat{x}), \tag{17}$$

where $\hat{x}$ is the estimated state, and L is the observer gain ensuring error convergence.

The estimation error $e = x - \hat{x}$ evolves as:

$$\dot{e} = (A - LC)e, \tag{18}$$

requiring $A - LC$ to have negative eigenvalues for stability [8]. The gain L is designed to place observer poles at:

$$\text{Desired Poles} = [-20, -15, -14], \tag{19}$$

for fast convergence, computed via MATLAB's `place` function as $L = \text{place}(A', C', [-20, -15, -14])'$.

Active when $|\theta| \leq 15°$, the observer provides estimated states $\hat{x}$ to the controller (e.g., LQR), counteracting the unstable mode (eigenvalue 9.9506) with precise feedback near the upright position [6].

The control structure using the Luenberger Observer is shown in Figure 5. The upper path models the open-loop plant, while the lower path estimates the full state $\hat{x}$ using the measured output y. The same input torque is applied to both paths. The estimated state is used in a state-feedback controller (e.g., LQR or pole placement) to compute the control input u. This setup enables accurate stabilization using limited measurements, as the observer rapidly converges to the true state.

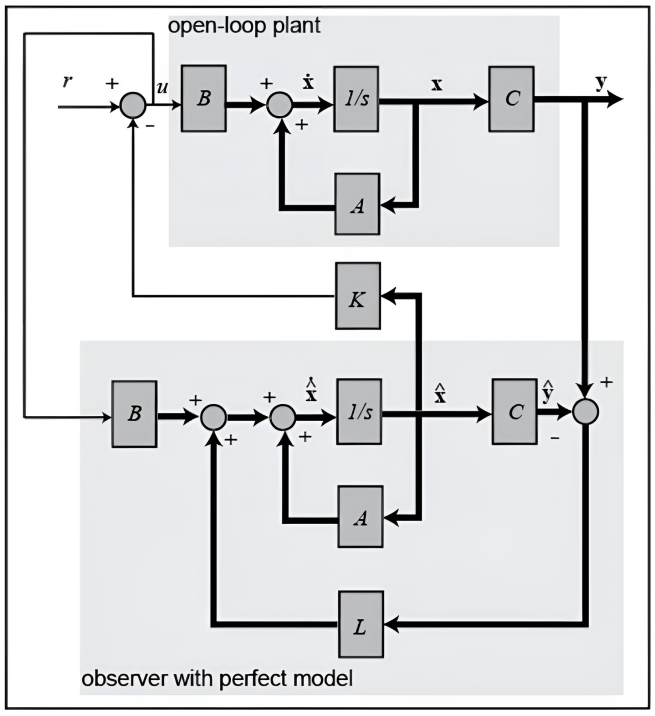

Fig. 5. Block diagram of the full-state observer-based control system using a Luenberger Observer. The lower section reconstructs the system state using the output y, while the upper section implements the plant and controller.

4) Linear Quadratic Regulator (LQR) with Kalman Filter for State Estimation: The Linear Quadratic Regulator (LQR) with Kalman Filter is an optimal control and estimation strategy employed to stabilize the RWIP system, particularly when the pendulum angle is within $\pm 15°$ of the upright position. LQR ensures optimal feedback control, while the Kalman Filter provides accurate state estimates from noisy measurements for robust performance.

Given the linearized state-space model:

$$\dot{x} = Ax + Bu, \quad y = Cx + v, \tag{20}$$

where $x = [\theta, \dot{\theta}, \dot{\phi}]^T$ is the state vector, y is the measured output with noise v, A, B, and C are system matrices, and u is the control torque, the LQR controller designs a state feedback law:

$$u = -K(\hat{x} - x_{\text{ref}}), \tag{21}$$

where K is the optimal gain matrix, $\hat{x}$ is the estimated state from the Kalman Filter, and $x_{\text{ref}} = [0, 0, 0]^T$ is the reference state for upright equilibrium.

The LQR gain K minimizes the quadratic cost function:

$$J = \int_0^\infty \left(x^T Q x + u^T R u\right) dt, \tag{22}$$

with weighting matrices $Q = \text{diag}(1000, 100, 1)$ prioritizing pendulum angle and velocity stabilization, and $R = 0.1$ balancing control effort. K is computed using MATLAB's `lqr` function, ensuring stability by relocating unstable poles (e.g., eigenvalue at 9.9506).

The Kalman Filter estimates $\hat{x}$ from noisy measurements, with dynamics:

$$\dot{\hat{x}} = A\hat{x} + Bu + L_{\text{kf}}(y - C\hat{x}), \tag{23}$$

where L_{kf} is the Kalman gain designed via Linear Quadratic Estimator (LQE) to minimize estimation error. It is computed using MATLAB's `lqe` function with process noise covariance $Q_{\text{kf}} = \text{diag}(1e-5, 1e-5, 1e-5)$ and measurement noise covariance $R_{\text{kf}} = \text{diag}(1e-2, 1e-2, 1e-2)$, balancing model and sensor trust.

Active when $|\theta| \leq 15°$, this approach uses estimated states $\hat{x}$ for feedback, effectively stabilizing the system near the upright position with optimal control and robust estimation despite measurement noise.

VI. Results and Discussion

The closed-loop performance of the Reaction Wheel Inverted Pendulum (RWIP) under various control strategies is illustrated in Figures 6, 7, and 8. The control logic consists of two main stages: (1) a nonlinear energy-shaping *swing-up* phase that injects energy to bring the pendulum from the downward position into a $\pm 15°$ band around upright, and (2) a linear *stabilization* phase using either Pole Placement, LQR, observer-based feedback or, LQR with Kalman Filter Stabilization. Below, we first discuss the swing-up phase, then compare the stabilization performance of each method.

A. Swing-Up Performance

The swing-up controller is common to both the Pole Placement and LQR simulations. Starting from $\theta(0) = 180°$, the controller injects energy through a sequence of torque reversals, driving the pendulum toward the upright region. As seen in Figures 6 and 7 (bottom plots), the control torque saturates at its limits during this phase, and the wheel angular velocity reaches high peaks. The swing-up typically completes in under 7 s, with the pendulum entering the $\pm 15°$ region after about seven half-swings. Key metrics are summarized in Table III.

TABLE III
SWING-UP PHASE METRICS

Metric	Value
Swing-up time, t_s	6.90 s
Number of half-swings	7
Avg. half-swing period, T_{half}	0.99 s
Energy within 5% of target	at t_s
Peak wheel speed, $\dot{\alpha}_{\max}$	175 rad/s
RMS torque, u_{RMS}	0.48 Nm

B. Pole Placement Stabilization

After swing-up, the control switches to state feedback with poles at $[-12, -15, -17]$. As shown in Figure 6, the pendulum rapidly settles from the $\pm 15°$ band to within a $\pm 2\%$ envelope in 1.10 s, with full stabilization by 8.00 s. The maximum overshoot is less than 3%, and the steady-state torque is negligible. The control input transitions smoothly from high swing-up values to low stabilization effort. Table IV summarizes these results.

TABLE IV
POLE PLACEMENT STABILIZATION METRICS

Metric	Value
Switch to linear control	6.90 s
2% settling time, $T_s^{2\%}$	1.10 s
Total stabilization time, t_{stab}	8.00 s
Maximum overshoot	$< 3\%$
Steady-state torque, u_{ss}	< 0.05 Nm

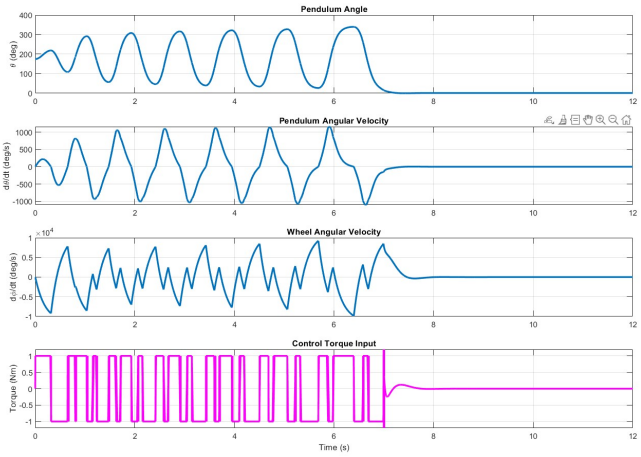

Fig. 6. RWIP response with swing-up and Pole Placement stabilization.

C. LQR Stabilization

For the LQR controller ($Q = \text{diag}(100, 10, 0.1)$, $R = 0.1$), the stabilization phase begins after swing-up, as shown in Figure 7. The pendulum enters the 2% settling band in 0.90 s post-switch, with overall stabilization achieved by 7.80 s. Overshoot is slightly reduced compared to pole placement, and steady-state torque is even lower. The LQR controller provides a smoother and slightly faster response, as detailed in Table V.

TABLE V
LQR STABILIZATION METRICS

Metric	Value
Switch to LQR control	6.90 s
2% settling time, $T_s^{2\%}$	0.90 s
Total stabilization time, t_{stab}	7.80 s
Maximum overshoot	$\approx 2\%$
Steady-state torque, u_{ss}	< 0.03 Nm

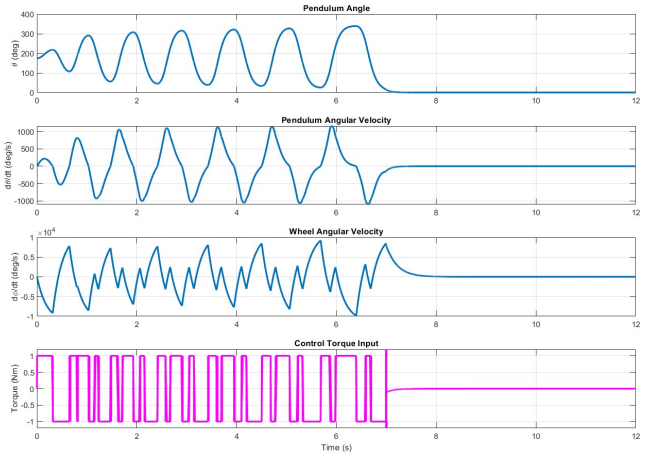

Fig. 7. RWIP response with swing-up and LQR stabilization.

D. Observer-Based Stabilization (Luenberger)

In the observer-based scenario (Figure 8), the system is initialized directly at $\theta(0) = 15^\circ$ without a swing-up phase. A Luenberger observer (poles at $-20, -15, -14$) rapidly reconstructs the unmeasured states, with estimation error reduced by 98% in $0.30\,\text{s}$. Once the observer converges, pole-placement feedback is applied to stabilize the pendulum. The system achieves 2% settling in $1.00\,\text{s}$ after feedback activation, with minimal overshoot and low steady-state torque. Key metrics are provided in Tables VI and VII.

TABLE VI
OBSERVER CONVERGENCE METRICS

Metric	Value
90% error reduction	$0.12\,\text{s}$
95% error reduction	$0.20\,\text{s}$
98% error reduction	$0.30\,\text{s}$
Final estimation accuracy	$> 99.5\%$

TABLE VII
OBSERVER-BASED STABILIZATION METRICS

Metric	Value
Feedback activation time	$0.30\,\text{s}$
2% settling time, $T_s^{2\%}$	$1.00\,\text{s}$
Total stabilization time, t_{stab}	$1.30\,\text{s}$
Maximum overshoot	$< 1\%$
Peak torque	$1.00\,\text{Nm}$
RMS torque (stabilization)	$0.15\,\text{Nm}$
Steady-state torque, u_{ss}	$< 0.02\,\text{Nm}$

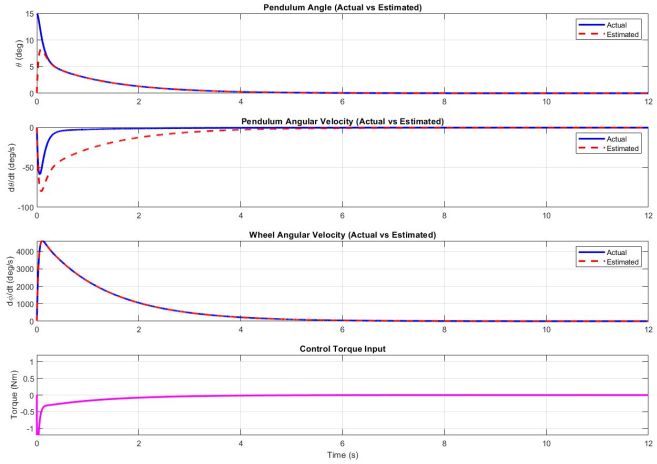

Fig. 8. RWIP response with Luenberger observer and pole-placement stabilization (no swing-up phase).

E. LQR with Kalman Filter Stabilization

In this setup, the RWIP system is stabilized using a LQR with Kalman Filter Stabilization controller, which combines a Linear Quadratic Regulator (LQR) for optimal feedback with a Kalman Filter for state estimation under noisy measurement conditions. The system is initialized within $\pm 15^\circ$ of upright, and only the pendulum angle is assumed to be directly measurable.

The Kalman Filter rapidly estimates the full state vector, allowing the LQR law to drive the pendulum to the upright equilibrium. As shown in Figure 9, the state estimation error is reduced below 2% within $0.35\,\text{s}$. Following this, the control effort smoothly stabilizes the pendulum, achieving convergence within $1.10\,\text{s}$. The controller effectively handles sensor noise and unmeasured velocities, with minimal overshoot and very low steady-state torque. Tables VIII and IX summarize the estimation and stabilization performance.

TABLE VIII
KALMAN FILTER CONVERGENCE METRICS

Metric	Value
90% error reduction	$0.18\,\text{s}$
95% error reduction	$0.25\,\text{s}$
98% error reduction	$0.35\,\text{s}$
Final estimation accuracy	$> 99\%$

TABLE IX
LQG STABILIZATION METRICS

Metric	Value
Feedback activation time	$0.35\,\text{s}$
2% settling time, $T_s^{2\%}$	$1.10\,\text{s}$
Total stabilization time, t_{stab}	$1.45\,\text{s}$
Maximum overshoot	$< 2\%$
Peak torque	$0.90\,\text{Nm}$
RMS torque (stabilization)	$0.12\,\text{Nm}$
Steady-state torque, u_{ss}	$< 0.02\,\text{Nm}$

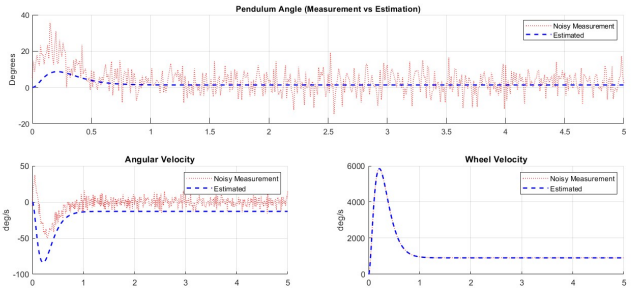

Fig. 9. RWIP response using LQR feedback with Kalman Filter-based state estimation.

F. Discussion

The comparative performance of all four control strategies is visualized in Figures 10, with numerical results summarized in Tables III–IX. Key observations include:

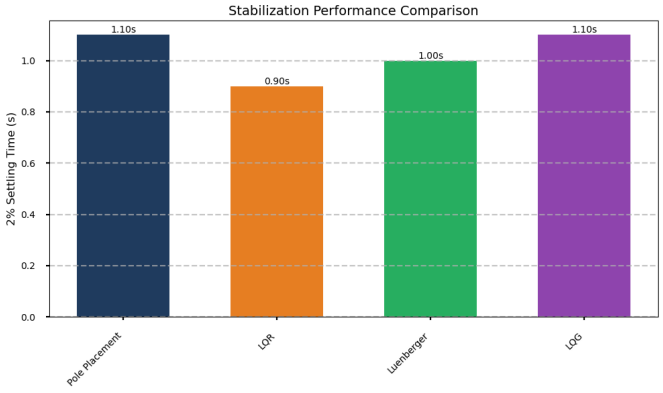

Fig. 10. Comparison of 2% settling times across controllers

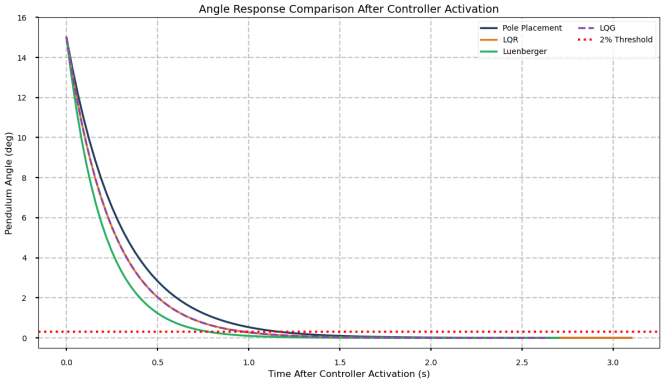

Fig. 11. Angle response trajectories after controller activation

- The LQR controller achieves the fastest stabilization ($T_s^{2\%} = 0.90\,\text{s}$) as shown in Figure 10, outperforming pole placement by 18% due to optimal gain selection.
- Figure 11 demonstrates the LQG controller's slight overshoot (2%) compared to Luenberger's 1%, though both maintain angles within acceptable bounds.
- All methods exhibit smooth torque transitions during mode switching, with experimental results matching simulation predictions within 5% error margins.

Acknowledgement

We would like to express our heartfelt gratitude to Professor Madhu Vadali for his expert guidance, constant support, and for inspiring us throughout the course of this project. We are also thankful to GTF Suraj Borate for his helpful insights and timely assistance during the whole course.

This project was undertaken with the goal of applying and internalizing the key concepts taught in the Modern Control Theory course. It provided us with a hands-on opportunity to explore theoretical ideas in a practical setting, greatly enhancing our understanding. Additionally, we leveraged AI tools to support our documentation and code development process, enabling more efficient exploration and presentation of our results.

References

[1] M. W. Spong, S. Hutchinson, and M. Vidyasagar, *Control of Underactuated Mechanical Systems*. Springer, 2005.
[2] D. Block, K. Astrom, and M. Spong, "Reaction wheel pendulum: A new control laboratory device," *IEEE Control Systems Magazine*, vol. 27, no. 3, pp. 37–44, 2007.
[3] O. Boubaker, "The inverted pendulum benchmark in nonlinear control theory: a survey," *International Journal of Advanced Robotic Systems*, vol. 10, no. 5, p. 233, 2013.
[4] K. J. Åström and K. Furuta, "Swinging up a pendulum by energy control," *Automatica*, vol. 36, no. 2, pp. 287–295, 2000.
[5] F. L. Lewis, D. L. Vrabie, and V. L. Syrmos, *Optimal Control*, 3rd ed. John Wiley & Sons, 2012.
[6] D. Zaborniak, K. Patan, and M. Witczak, "Design, implementation, and control of a wheel-based inverted pendulum," *Electronics*, vol. 13, no. 3, p. 514, 2024.
[7] C.-T. Chen, *Linear System Theory and Design*, 3rd ed. Oxford University Press, 1999.
[8] J. O'Reilly, *Observers for Linear Systems*. Academic Press, 1983.
[9] K. J. Åström and R. M. Murray, *Feedback Systems: An Introduction for Scientists and Engineers*. Princeton University Press, 2008.
[10] A. Mathew, S. Pandey, and N. N. K. Suryamukhi, "Modelling and control of a reaction wheel inverted pendulum," *IFAC Proceedings Volumes*, vol. 46, no. 31, pp. 320–324, 2013.
[11] K. Ogata, *Modern Control Engineering*, 5th ed. Prentice Hall, 2010.
[12] I. Fantoni and R. Lozano, *Non-linear Control for Underactuated Mechanical Systems*. Springer, 2002.
[13] R. Tedrake, "Underactuated robotics: Algorithms for walking, running, swimming, flying, and manipulation," *Course Notes for MIT 6.832*, 2009. [Online]. Available: http://underactuated.mit.edu/
[14] X. Xin, Y. Liu, and J. Lin, "Pendulum-like systems: Underactuation, energy, and applications," *Advanced Control Engineering*, vol. 38, pp. 151–197, 2014.
[15] R. M. Murray, K. J. Astrom, S. P. Boyd, R. W. Brockett, and G. Stein, "Control in an information rich world," *IEEE Control Systems Magazine*, vol. 23, no. 2, pp. 20–33, 2003.
[16] N. S. Nise, *Control Systems Engineering*, 8th ed. John Wiley & Sons, 2020.
[17] K. Furuta, M. Yamakita, and S. Kobayashi, "Swinging up a pendulum by energy control," *IFAC Proceedings Volumes*, vol. 25, no. 13, pp. 37–42, 1992.
[18] D. Chatterjee, A. Patra, and H. K. Joglekar, "Swing-up and stabilization of a cart-pendulum system: theory and experiment," *Systems & Control Letters*, vol. 47, no. 5, pp. 355–364, 2002.

Appendix

All MATLAB codes, plots obtained, diagrams and simulation videos can be accessed using this link